

CORRECTION OF SHADOWING IN IMAGING SPECTROSCOPY DATA BY QUANTIFICATION OF THE PROPORTION OF DIFFUSE ILLUMINATION

Daniel Schläpfer^a, Rudolf Richter^b, Alexander Damm^c

^a ReSe Applications Schläpfer, Langeeggweg 3, CH-9500 Wil, Switzerland; daniel@rese.ch

^b German Aerospace Center, DLR, Wessling, Germany; Rudolf.Richter@dlr.de

^c Remote Sensing Laboratories, University of Zurich, Switzerland; adamm@geo.uzh.ch

KEY WORDS: atmospheric correction, irradiance, illumination, cast shadow correction, vegetation indices.

ABSTRACT:

High spatial resolution imaging spectroscopy data is affected by various shadowing influences: be it the shadows of buildings, within forests, at forest borders, by single trees, by terrain, or by clouds. The radiometric performance of modern imaging spectroscopy systems provides a dynamic range which is large enough to retrieve useful spectral surface information even within full cast shadows. Thus, atmospheric correction routines should provide a capability to account for all above-mentioned types of cast shadows. The use of accurate surface models for cast shadow ray tracing does not lead to useful results in many cases as the surface representation with respect to the radiometry is never accurate enough. Therefore, an image-based method applicable to a broad variety of image data is searched.

A method for cast shadow detection and correction has been implemented and included in the workflow of the ATCOR atmospheric compensation package. The shadows are retrieved from calibrated at-sensor radiance imagery relying on the fact that all areas in shade are illuminated by a large proportion of diffuse irradiance. The diffuse irradiance is caused by scattering in the atmosphere and thus exhibits very specific spectral characteristics compared to the direct irradiance. Specifically, the relative signal in the blue is significantly higher in areas affected by cast shadow than in directly illuminated regions. Specific indices have been defined to quantify the shadow fraction on a per-pixel basis by exploiting the spectral properties of illumination. This strategy results in a continuous quantification of the shadow field. The output is used directly in the atmospheric/topographic correction on the basis of the ATCOR model in a physical way.

Tests of the procedure on various imaging spectroscopy data samples show significant improvements of surface reflectance products in forests and in urban areas. Validation results demonstrate the performance and indicate limitations of the proposed methods. Implications for the retrieval of remote sensing products are discussed, with a particular focus on the vegetation indices normalized difference vegetation index (NDVI) and photochemical reflectance index (PRI).

1. INTRODUCTION

The ultimate goal of atmospheric compensation is the derivation of spectral albedo products from calibrated at sensor radiances. Many aspects of the atmospheric compensation problem have been solved and are readily available in atmospheric correction methods such as ATCOR (Richter and Schläpfer, 2002). The ATCOR model also contains the ability to correct data in terrain by calculating the irradiance field on a per pixel level. The direct irradiance component is calculated by the standard cosine law taking all atmospheric effects into account. The diffuse irradiance is simulated on the basis of the atmospheric scattering processes including the portion of the visible skyview and the backscattered radiation from adjacent pixels (i.e. the adjacency effects). In shadowed areas, modeling of the diffuse irradiance is of high importance as it is the only illumination source in such cases (Richter and Müller, 2006). If the simulation of the irradiance field is accurate, a correction of the image data is feasible with high accuracy given two further preconditions: First, the image data has to be of an enhanced accuracy level in terms of absolute calibration but also concerning its dynamic range. Second, continuous shadow fractions must be accurately identified in the imagery. Modern radiometric airborne scanners fulfill the first requirements in both dynamic range and calibration accuracy. However, the quantitative detection of shadow fractions is still challenging and a significant source of uncertainty.

For low spatial resolution imagery, cast shadows are often derived using a ray tracing algorithm on a digital elevation model. This method is not applicable for high resolution imagery at spatial resolutions below 5 meters as tree crowns are not appropriately radiometrically represented by digital elevation data – even if high resolution LIDAR data is taken as reference. Thus, image based methods for shadow detection must be used. By its nature, the shading effect is a continuous parameter which can not be characterized by a shade/no-shade classification. A quantitative method is therefore essential for derivation of the relative shade intensity. Such results can be used for subsequent radiometric and atmospheric correction.

Currently, shadow detection methods have been implemented and used for high resolution imagery, for the detection of cloud shadows and shadows from buildings (Davenport and Ressl 1999, Alder-Golden et al. 2002, Asner 2003, Shao et al. 2011). Some empirical training of the method is, however, often required but then the methods would also work also on non-calibrated data (Bochow et al., 2011). Colour transformation routines are an alternative approach and sometimes applied, but are of pure empirical nature (Liu and Fang 2002, Zhu and Woodstock 2012), or the methods are restricted to selected targets (Mayer et al., 2004).

The goal of this contribution is to propose a robust shadow quantification method which is directly applicable to calibrated at-sensor radiance imagery. The intrinsic radiometric properties of shadowed areas due to their specific illumination shall be evaluated. The method uses the radiometric properties of diffuse illumination for the quantification of shadows without any image-based training, sampling, or statistical adaption. This is an important precondition for the method to be applicable in operational processing environments. A detailed assessment of the impact of varying fractions of direct and diffuse illumination when not considered in atmospheric correction approaches is provided. This analysis is based on simulated and real data and focuses on reflectances and subsequently derived vegetation products.

2. SENSITIVITY ANALYSIS

Artificial test data on the basis of ground reflectance data has been prepared to develop the baseline of the shadow detection method. Two sets of reflectance spectra have been selected for the simulation of spectral behavior in response to varying fractions of direct to diffuse irradiance:

- the JHU library of man made and natural materials (available within the ENVI™ software)
- a series of ProSAIL simulations (Jacquemoud et al., 2009) for two vegetation densities (LAI=1 and LAI=4) and variable chlorophyll contents (10-80 $\mu\text{g cm}^{-2}$).

The surface reflectance data contained in these two data sets are propagated to at sensor radiances using a simplified radiative transfer formulation as used in the ATCOR top of atmosphere calculation module using the ATCOR Look Up Tables derived from MODTRAN5 (Berk et al. 2004). The fractional shading (fraction of direct irradiance) is varied between 0 and 100% in steps of 1%. A 30 degree solar zenith angle and a clear sky visibility of 40 km, a ground elevation 0.5 km and a flight altitude of 2 km are assumed for the simulations. Figure 1 depicts the resulting at-sensor radiance spectra in steps of 10% shading for a subset of materials. The simulation is done for the high spectral resolution Hypspe VNIR instrument (Baarstad et al. 2006, Lund 2013). Almost all objects show less variation in the blue spectral band compared to the red band. The diffuse irradiance is increasing towards lower wavelengths which results in a less visible signature of shading at those wavelengths. The signature of ‘shade’ is depicted by plotting the spectra relative to a fixed wavelength in the red at 669 nm (right section of Figure 1).

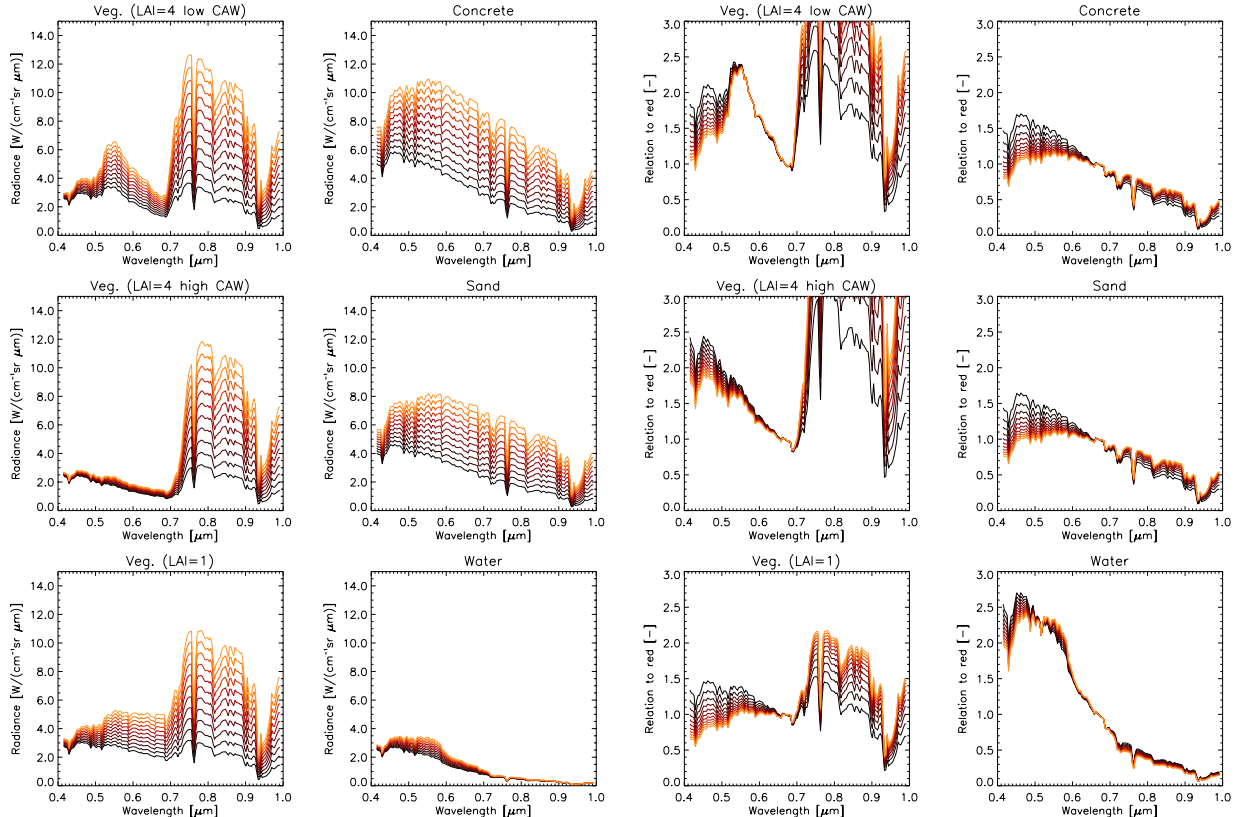


Figure 1 Simulated at-sensor radiances for six selected ground reference targets at varying shading between 100% (black curve) and full illumination (orange curve) at 30 degrees solar zenith. Left part: at-sensor radiance; right part: radiance ratio (L/L_{red}) relative to red spectral band at 669 nm.

The exact fractions of diffuse and direct irradiance have to be considered in atmospheric correction calculations. If neglected, strong artifacts occur in retrieved reflectances and subsequently derived remote sensing products (e.g., vegetation indices). Figure 2 shows the effect of varying shadow fractions on reflectances derived from common atmospheric correction approaches assuming a constant ratio of direct and diffuse irradiance. The strong variation of radiances caused by shadowing (Figure 1) directly propagates in derived reflectances. For concrete and vegetation, for example, highest underestimations occur in the near infrared (up to 74%) in fully diffusely illuminated areas, for water targets highest underestimations of reflectance were found in the green spectral region with values up to 52%.

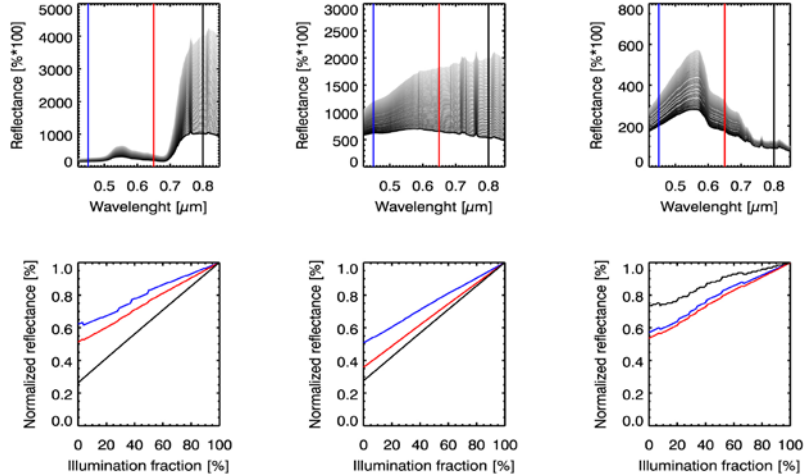


Figure 2: Impact of varying fractions of direct irradiance on reflectance spectra derived from atmospheric correction considering a constant ratio of diffuse to direct irradiance. Three surface types were analyzed, i.e., vegetation (LAI=4, Chl=30 $\mu\text{g cm}^{-2}$) (left), concrete (middle), and water (right). The upper panels show the gradient of reflectances from direct illuminated surfaces (grey) to fully shaded surfaces (black). The lower panels show the dependency of selected reflectances (blue 0.45 μm , red 0.64 μm , nir 0.8 μm) on the shadowing fraction.

3. SHADOW QUANTIFICATION METHOD

Shadow detection is not easily feasible by physical inversion due to two reasons: i) the shadow signature is a function of diffuse illumination which itself depends on the neighboring image area, ii) the variations of ground reflectance may not be discernible from the atmospheric signature: e.g., the density of vegetation significantly affects the spectral curve of the relevant spectra in the blue-to-red spectral range. To account for both effects, empirical measures are searched to get, if combined, a probability of shadowing for each pixel or with other words the individual fractions of diffuse and direct irradiance. Our tests have shown that linear unmixing methods or spectral angle mapping do not lead to a successful consistent quantification of the irradiance field. It has therefore been decided to rely on an index-based 4-band method only. This has the advantage that the method can be applied to hyperspectral and multispectral imagery in the same way. The selected bands are located at 460, 550, 670, and 780 nm – if these wavelengths are not available the closest bands are selected automatically in the method (as long as the useful range between 450 and 800 nm is covered, at least). An ideal shadow quantifier index based on these bands should fulfill the following conditions:

- The output data range is the same for typical natural and artificial targets
- The index is significantly increasing with illumination
- The index should be centered at about 0.5 to allow for a quantification of shadows between 0 and 1.

Using the simulated data, indices have been identified by a systematic evaluation of potential band combinations with respect to their sensitivity to quantify the amount of shading. After selecting the indices, empirical scaling factors for the proposed indices have been derived using this simulated data. The indices were further refined by applying them to the test images described in the subsequent section. It has been found that using a 4-band configuration provides a reliable way for shadow detection with some restrictions as described later in this paper. The proposed method for a continuous quantification of direct illumination combines the four bands in three indices as described hereafter.

3.1 Red-NIR Brightness (RN)

The apparent near infrared (NIR) and the red at-sensor reflectance are suited for the quantification of the pixel brightness. The red-NIR brightness (RN) is calculated from calibrated imagery by taking the minimum apparent reflectance of the NIR and the red spectral band:

$$\rho_{RN} = \min \left[\frac{\pi L_{NIR}}{E_{0,NIR} \cos(\theta_0)}, \frac{\pi L_{red}}{E_{0,red} \cos(\theta_0)} \right],$$

where L_{NIR} and L_{red} are the at-sensor radiances, E_0 is the top of atmosphere solar irradiance and θ_0 is the solar zenith angle. The RN Brightness is used to quantify very dark shadows in order to avoid instabilities of the other indices due to the decreased SNR at low signals. On the other hand, the NIR apparent reflectance (first part of RN) is used for the detection of water and dark objects and to weight the two subsequent indices for low apparent reflectance targets (e.g., water).

3.2 Red-Blue Relation (RB)

The diffuse illumination is characterized by increased radiance levels towards shorter wavelengths due to Rayleigh scattering in the atmosphere (i.e., blue sky illumination) and the higher aerosol scattering at shorter wavelengths. This fact can be used to quantify the shading of an object. A simple index between red and the blue spectral bands is directly related to the shading for most surfaces. Its absolute value, however, varies with the surface type. Specifically, vegetation has a very different spectral shape in the visible part of

the spectrum compared to non-vegetated areas. Therefore, the blue-red ratio has to be adjusted for the amount of vegetation, which correlates the by the NIR radiance. Thus, an NIR-adjusted red blue index (RB) is proposed to quantify the shading effect:

$$K_{RB} = 0.7 \cdot \left(\frac{L_{red} + 0.1 \cdot L_{nir}}{L_{blue}} \right).$$

The additive term L_{nir} corrects for variations of absorption in the red band which is mainly determined by chlorophyll in case of vegetation surfaces. The factor of 0.1 has been found empirically from analysis of a series of vegetation spectra and makes this index consistent across a wide range of different vegetation types with varying LAI and chlorophyll content. Furthermore, a scaling of 0.7 is applied to adjust to a mean value of approximately 0.5 of this index for typical targets, a condition defined above.

3.3 Green-Red-Blue Extrapolation (GRB)

A third index is introduced to quantify shadows on surface types which are not well characterized by the RB-index. This index shows a better responsivity e.g. for water, snow, asphalt or dark concrete. A linear ground reflectance spectrum is assumed for such spectra. The green-red curve is extrapolated to the blue to obtain an estimate of relative variation of the blue radiance:

$$K_{GRB} = 1.25 \cdot \left(\frac{L_{green} - b(\lambda_{green} - \lambda_{blue})}{L_{blue}} - 0.8 \right), \quad \text{where } b = \frac{L_{red} - L_{green}}{\lambda_{red} - \lambda_{green}}.$$

The scaling factor of 1.25 is required to this three-band GRB-index to adjust dark water targets to the range expected by the RB index.

3.4 Combination

To correct any surface type, the above mentioned indices have to be combined into one shadow fraction index considering following logics:

- shades are dark in the NIR, and even darker for water, but occasionally relatively bright on snow.
- for all targets, the red-blue index increases with illumination (but on differing levels)
- for non-vegetation and water the GRB index increases depending on brightness

Some empirical analysis has been required to find an optimum combination – it has been found that the RB index serves as a stable shadow quantifier in most cases. It only needs to be adjusted for very bright and very dark objects. A combined index is thus created which is defined between 0 for cast shadows and 1 for illuminated areas. The shadow thresholds are typically between 0.4 for full cast shadows and 0.6 for fully illuminated areas.

The combination steps are as follows:

1. The RB index is used as the major shading quantifier.
2. The RB index values are adjusted for very dark objects by multiplication with the RN brightness. The RN brightness is scaled from 0 to 1 for reflectances between 0% and 2.5%, means the red-blue index of objects below 2.5% reflectance is scaled down to smaller values to enable their identification as shadow.
3. Dark surfaces (mainly water) with less than 2-4% apparent reflectance in the NIR are treated separately. For such surfaces, the GRB index is multiplied by a factor of two instead of using the RB index because the RB index is not sensitive enough on water surfaces,
4. The RB index for snow, which is quantified if the apparent reflectance exceeds 35-55% in the blue spectral band, is replaced by the GRB index and multiplied by a scaling factor to correctly quantify shadows on snow.

In order to keep the overall index continuous, transition ranges as indicated are used between the RB index and the GRB index for the dark and bright object, where the two indices are linearly weighted against each other according to the brightness.

4. APPLICATION TO SIMULATED DATA

The shadow detection index has been applied on the two simulated test data sets (refer to section 2). The resulting continuous shadow mask was then used as input for an atmospheric correction to parameterize varying fractions of diffuse and direct illumination. Resulting reflectances and subsequently derived vegetation indices (i.e., NDVI, PRI) are evaluated to assess the performance of the proposed shadow correction method and to reveal its limitations.

4.1 Shadow Fraction Index Simulations

The individual three and the combined index applied on the simulated spectra are shown in Figure 3. The combined index responds similar across the range of illumination fractions for both vegetation and non-vegetated areas. For some bright and artificial targets and on sparse vegetation, however, the combined index behaves differently. In particular the divergence between different vegetation types is obvious and will need further analysis. The chosen solution is clearly a compromise for all surface types in commonly occurring in a typical Mid-European scene. For other settings the set of indices must be adapted otherwise the index range might vary. Alternatively, the proposed index may have to be optimized for vegetation to get to a better overall result.

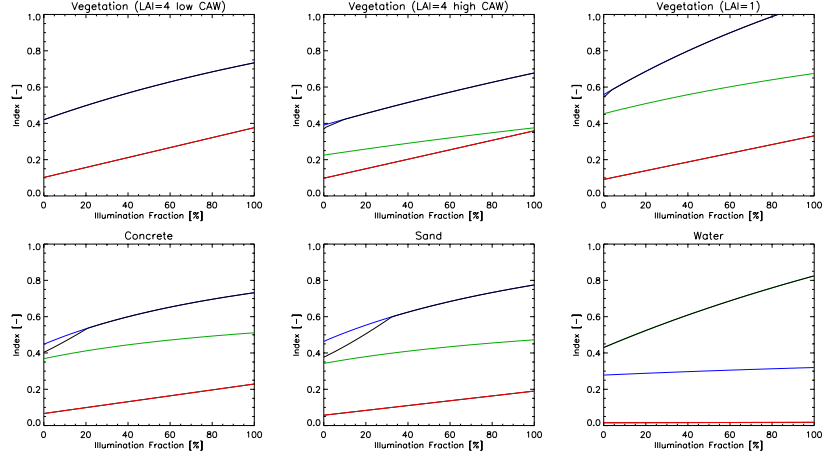


Figure 3: Shading index combination for various simulated at-sensor radiances. Red: NIR apparent reflectance, blue: blue-red index, green: blue-red-green index, black: index combination.

4.2 Evaluation of Products on Simulated Data

An analysis of derived reflectances and vegetation products (i.e., the simple vegetation indices NDVI and PRI) was carried out to evaluate potential improvements when pixel wise fractions of diffuse and direct irradiance are considered in atmospheric correction routines. The simulated radiances were atmospherically corrected using the ATCOR-4 code and the bottom-of-atmosphere directional reflectances were derived. The atmospheric correction used a variable fraction of diffuse and direct irradiance based on the continuous shadow mask, while keeping the other ATCOR input parameters as used for the forward simulation (e.g., for the water vapor amount, the aerosol load, the sensor type, or the geometric assumptions).

Figure 4 shows the resulting reflectances of three surfaces with varying amount of direct irradiance. Compared to the uncorrected data (Figure 2), a significant decline of reflectance variability is obvious. The analysis, however, also reveals current limitation of the continuous shadow detection. Only very high shadow fractions can be reliably quantified, whereas low to intermediate shadow fractions are not properly quantified and cause over- and underestimations in calculated reflectance signals.

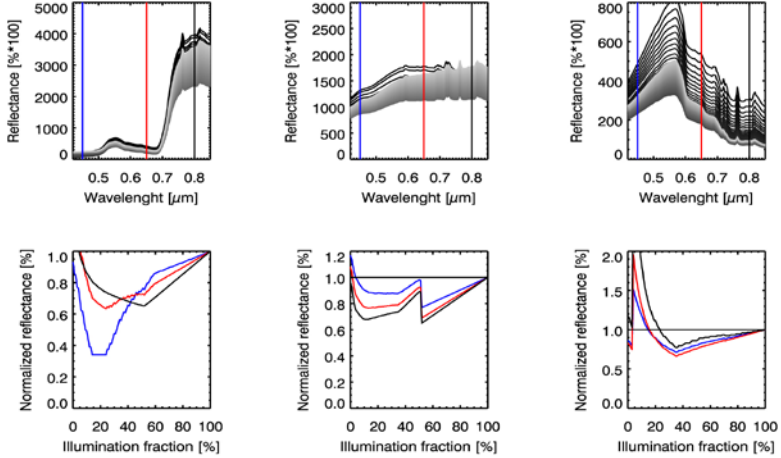


Figure 4: Impact of varying fractions of direct irradiance on reflectance spectra derived from atmospheric correction considering a variable ratio of diffuse to direct irradiance. The upper panels show the gradient of reflectances from direct illuminated surfaces (grey) to fully shaded surfaces (black). The lower panels show the dependency of selected reflectances (blue 0.45 μm, red 0.64 μm, NIR 0.8 μm) on the shadowing fraction.

The analysis of simple vegetation products, i.e., the NDVI and the PRI, reveals an improvement of data quality when changing fractions of diffuse and direct irradiance are considered during atmospheric correction (Figure 5). The NDVI derived from uncorrected data for sparse vegetation canopies (LAI=1) varies up to 30% in response to changing illumination conditions. The correction reduces this variation up to 5%. The improvement is even better for dense vegetation canopies (up to 10%). More important, the NDVI is rather constant across the gradient of shadow fractions. Only a slight improvement can be achieved for the PRI for dense canopies. In case of sparse canopies, the correction introduces a higher PRI variability across the range of shadow fractions after the shadow correction was applied (data is not depicted here).

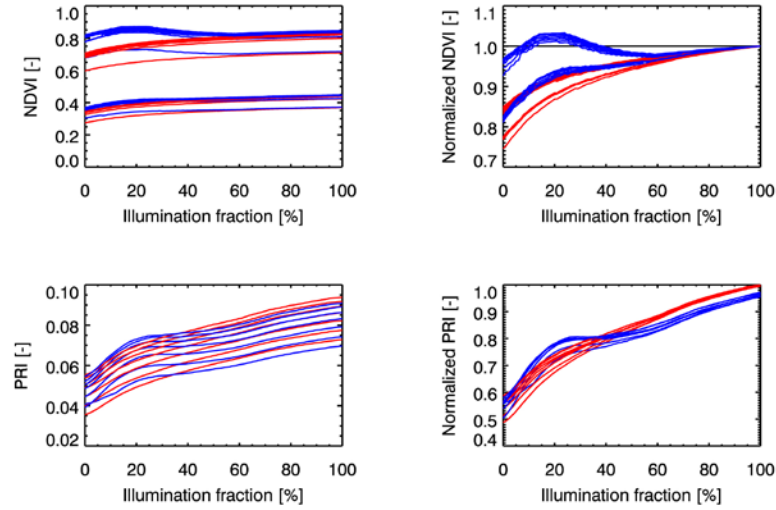


Figure 5: Impact of illumination on vegetation products before (red lines) and after (blue lines) the shadow correction.

5. APPLICATION TO IMAGE DATA

In view of atmospheric correction, the shadow detection routine is applied to a selection of imagery and the impact on the two selected standard vegetation products is evaluated.

5.1 Shadow Detection Results

The Leica multispectral airborne digital photogrammetric scanner (ADS-80; Sandau et. al. 2000) has been selected to demonstrate the applicability of the developed method also for multispectral as a standard 4-band combination is sufficient for shadow quantification. Figure 6 shows an example of the ADS image. A limit of 0.3 for full shadow and 0.5 for no shadow has been set to the shading index for this analysis. The shadows are identified correctly even at the high spatial resolution of 0.25m of this instrument. Problems occur at shadow borders which may get widths of up to 3-5 pixels, specifically for long-range terrain shadows.

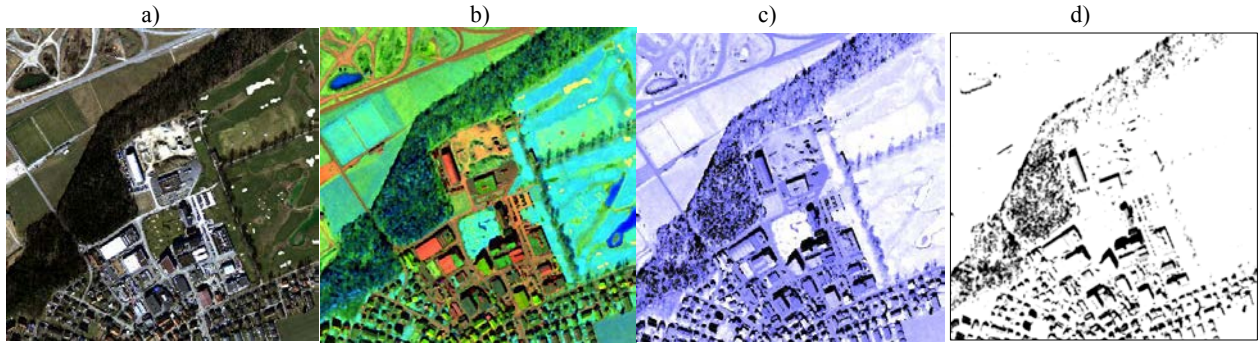


Figure 6 ADS data shadow quantification, from left to right: a) RGB original image; b) RGB composite of three indices (R: Brightness, G: Red-Blue, B: Green-Blue); c) combined index; d) shadow mask after applying threshold limits.

The same index is then applied to Hypslex imagery (Lund 2013), acquired in Norway in July 2011 at a zenith angle of 26 degrees from a flight altitude of 1450 m above ground and 0.5 m nominal resolution. The shadow detection was mostly feasible despite some dark asphalt areas which were very sensitive to the shadow detection routine. Some fine-tuning of the indices helped to improve the method for this type of images as depicted in Figure 7. Still, the correction led to some shadow border artifacts which need further investigation.

Last, the method has been applied to two APEX data sets (Itten et. al. 2006) acquired over the city of Zurich, Switzerland, in June 2011 and the city of Wettingen, Switzerland, in June 2012. The two data sets have been flown at altitudes of about 6000m and 4100m above ground at solar zenith angles of 38 and 27 degrees, respectively. Using very similar threshold limits as for the other two systems (deviating not more than 20% after fine tuning), the shadows were correctly identified (compare Figure 8). It is relevant to note that the method performed well also on water and in difficult city environments. These results show a stable performance of the method for the selected range of images.



Figure 7 Application of method to HYSPEX sample data containing dark concrete and roof materials; left: RGB composite, middle: composite of three indices (as of Figure 6), right: shadowing after application of threshold.



Figure 8 Application of method to APEX sample data ‘Zurich City’ containing dark concrete and roof materials; same series of images as of Figure 7

5.2 Atmospheric Correction

Using the described continuous cast shadow map, the atmospheric correction routine ATCOR-4 is applied to the test images as depicted in Figure 9. The shading quantification layer is introduced directly to the code in combination with the image and the meta information. After the standard correction, the borders of shaded areas often appear over- or under-corrected which is visible as black or bright shadow borders. A shadow border correction routine has therefore been applied. This method calculates a brightness correction factor in direct vicinity to the cast shadow borders which can be identified from the cast shadow classification map using a buffering technique.

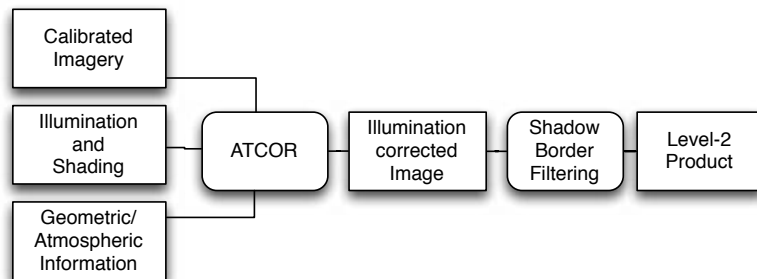


Figure 9: Illumination shading based atmospheric correction workflow.

Two examples of the atmospheric correction using image based shadows for the APEX system are shown in Figure 10. Some artifacts at the shadow borders are obvious and indicate an imperfect correction. Further improved shadow border filtering techniques are required. Figure 11 shows an example on the implications of the proposed method on measured top-of-canopy reflectance spectra. The depicted spectra show that the comparability of the spectra within the shadowed regions to the spectra outside of the shadows has been improved, pointing at possible improvements for quantitative analyses.

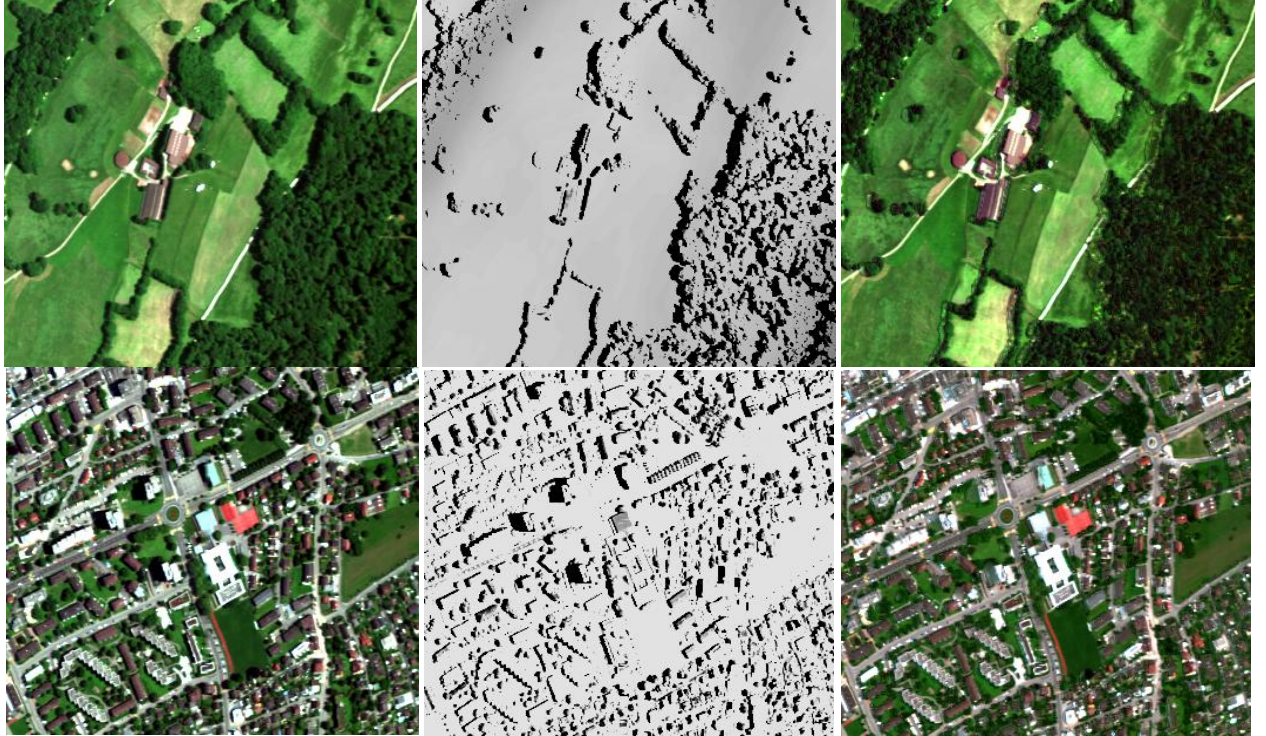


Figure 10: Shadow based atmospheric correction sample for two subsets of APEX imagery. Left: original RGB image. Middle: cast shadow map. Right: image after shadow correction.

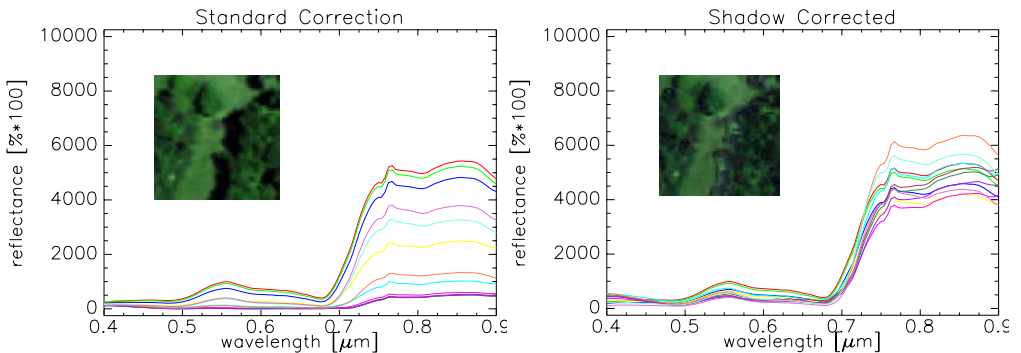


Figure 11: Spectra in a horizontal transect with and without shadow correction. The transect has been taken on a horizontal line across the shadowed area in the picture shown with the graph.

5.3 Validation on Product Level

A performance assessment of the method has been carried out by investigating the vegetation indices NDVI and PRI. Figure 12 shows that the consideration of changing fractions of direct and diffuse irradiance in atmospheric correction approaches significantly reduces shadowing effects on product level. Without such corrections, the variability of vegetation indices is mostly driven by the illumination instead of vegetation properties. After the correction, this sensitivity disappears and the vegetation products depict more realistic vegetation properties.

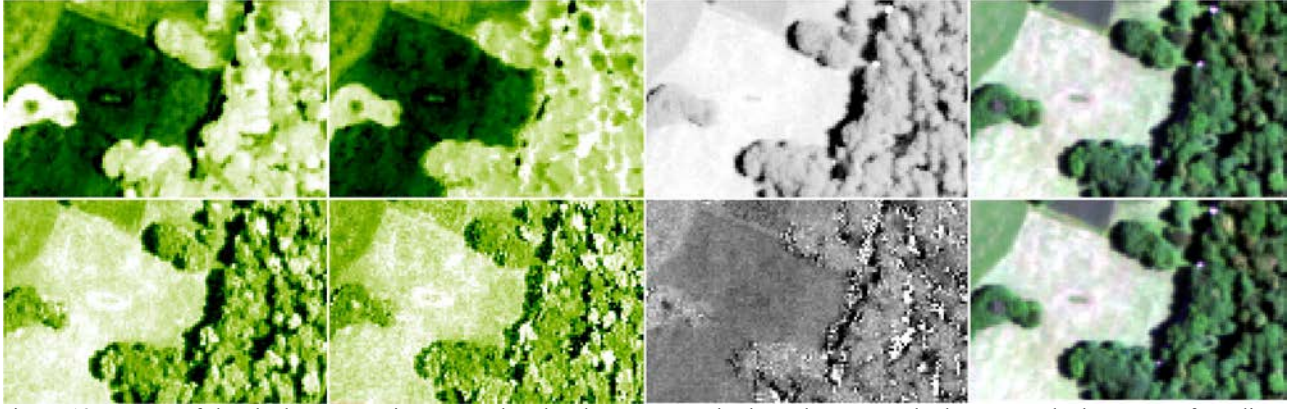


Figure 12: Impact of the shadow correction on product level. Upper panels show the NDVI, the lower panels the PRI. Left: Indices calculated on the uncorrected reflectances. Left-middle: Indices based on shadow corrected reflectances. Right-middle: Difference map between uncorrected and corrected indices. Right: True color image.

The observed minimized sensitivity of NDVI and PRI for shadowing effects is supported by a comparison of index values against a brightness estimate (Figure 13). Within a forested area with some clearings and supporting roads, the correlation between the NDVI and the brightness map decreases after the shadow correction from $R^2 = 0.29$ to $R^2 = 0.02$. For the PRI a more significant de-correlation could be observed (i.e. $R^2 = 0.42$ to $R^2 = 0.07$). It has to be noted that the correction changes the absolute values and the value range of PRI.

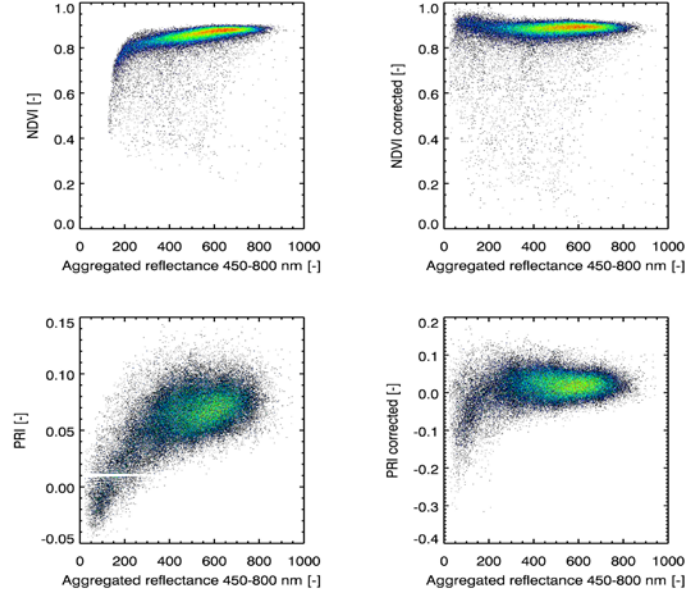


Figure 13: Relationship between NDVI (upper panels) and PRI (lower panels) and a brightness estimate for uncorrected (left panels) and corrected (right panels) data.

6. CONCLUSIONS AND OUTLOOK

A semi-empirical unsupervised analytical approach has been developed to continuously quantify shading in multispectral and hyperspectral imagery. The estimated shadow fractions were incorporated in atmospheric correction approaches of imaging spectroscopy data. The developed method has been tested on a selection of airborne imagery including the Hypslex and the APEX system, but also on the multispectral ADS-80 airborne system. Shadows were detected consistently. However, the thresholds for shadow detection had to be slightly adjusted depending on the system, calibration, and atmospheric conditions. One critical point is the accurate discrimination of water and shaded water from other dark objects (e.g., dark asphalt). This is considered as important for a good overall accuracy of atmospheric compensation. However, if the application is focused on vegetation analysis, distortions over water areas are less important. For spectroscopic data, further efforts could be made to pre-classify non-shaded areas as part of the shadow detection routines which would lead to better results.

The shadow correction is an important step towards spectral albedo data using physical modeling only. The described method is now available for operational use in the ATCOR programs. Still, these outputs are of directional nature and depend on the directionality of the illumination field. Currently, methods of model based BRDF correction are evaluated to be included as well in the radiometric processing workflow. This would help to finally deliver bi-hemispherical spectral albedo products after a complete atmospheric compensation.

7. ACKNOWLEDGEMENTS

This work has been supported by the Swiss Federal Office of Topography (swisstopo) which is gratefully acknowledged.

REFERENCES

- Adler-Golden, S., Matthew, M., Anderson, G., Felde, G., & Gardner, J. (2002). "An algorithm for de-shadowing spectral imagery. Presented at the 11th Airborne Earth Science Workshop, JPL, Pasadena, pp 8.
- Asner, Gregg, "Canopy shadow in IKONOS satellite observations of tropical forests and savannas," *Remote Sensing of Environment*, vol. 87, no. 4, pp. 521–533, Nov. 2003.
- Baarstad, I., Løke, T., & Kaspersen, P. (2006). "ASI – A New Airborne Hyperspectral Imager". Proceedings of 4th EARSeL Workshop on Imaging Spectroscopy., pp. 4.
- Berk A. , Gail P Anderson, Prabhat K Acharya, Lawrence S Bernstein, Leonid Muratov, Jamine Lee, Marsha J Fox, Steven M Adler-Golden, Jr. James H Chetwynd, Michael L Hoke, Ronald B Lockwood, James A Gardner, Thomas W Cooley, and Paul E Lewis, "MODTRAN5: a reformulated atmospheric band model with auxiliary species and practical multiple scattering options," in Proc., Sylvia S Shen and Paul E Lewis, Eds. 2004, pp. 341–347, SPIE.
- Bochow, M., Rogass, C., Peisker, T., Heim, B., Bartsch, I., Segl, K., & Kaufmann, H. (2011). "Automatic shadow detection in hyperspectral VIS-NIR images". Presented at the Proceedings of the 11th Earsel Imaging Spectroscopy Workshop, Edinburgh, pp 9.
- Davenport, M., & Ressl, W. (1999). "Shadow Removal in Hyperspectral Imagery". Presented at the International Symposium on Spectral Sensing Research, Las Vegas, Nevada.
- Jacquemoud, S., Verhoef, W., Baret, F., Bacour, C., Zarco-Tejada, P. J., Asner, G. P., et al. (2009). "PROSPECT+SAIL models: A review of use for vegetation characterization". *Remote Sensing of Environment*, 113(S1), S56–S66. doi:10.1016/j.rse.2008.01.026.
- Itten, K., Dell Endice, F., Hueni, A., Kneubühler, M., Schläpfer, D., Odermatt, D., et al. (2008). "APEX - the Hyperspectral ESA Airborne Prism Experiment". *Sensors*, 8(10), 6235–6259.
- Liu, J., Li, D., & Fang, T. (2012). "Shadow detection for color remotely sensed images based on multi-feature integration". *Journal of Applied Remote Sensing*, 6(1), 063521. doi:10.1117/1.JRS.6.063521.
- Lund, V. (2013, March 20). "HySpex -High Resolution, High Speed, Hyperspectral Cameras for Laboratory, Industrial and Airborne Applications". Lorenskog, Norway: Norsk Elektro Optikk AS. Retrieved from http://www.hyspex.no/pdfs/HySpex_general.pdf. pp 8.
- Mayer, R., Antoniades, J., Baumback, M., Chester, D., Edwards, J., Goldstein, A., D. Haas, and S. Henderson (2007). "Shadowed object detection for hyperspectral imagery" Presented at the Infrared Spaceborne Remote Sensing and Instrumentation XV, SPIE Vol. 6678, pp. 66780L–66780L–11. doi:10.1117/12.738408.
- Richter R. and Schläpfer D., "Geo-atmospheric processing of airborne imaging spectrometry data. Part 2: Atmospheric/Topographic Correction," *International Journal of Remote Sensing*, vol. 23(13), pp. 2631–2649, 2002.
- Richter, R., & Müller, A. (2005). "De-shadowing of satellite/airborne imagery". *International Journal of Remote Sensing*, 26(15), 3137–3148. doi:10.1080/01431160500114664.
- Sandau R., B Braunecker, H Driescher, A Eckardt, S Hilbert, J Hutton, W Kirchhofer, E Lithopoulos, R Reulke, and S Wicki, "Design Principles of the LH Systems ADS40 Airborne Digital Sensor," *IAPRS*, vol. XXXIII, no. Part B1, pp. 258–265, 2000.
- Shao Y., Gregory N Taff, and Stephen J Walsh, "Shadow detection and building-height estimation using IKONOS data," *International Journal of Remote Sensing*, vol. 32, no. 22, pp. 6929–6944, Nov. 2011.
- Zhu, Z., & Woodcock, C. E. (2012). "Object-based cloud and cloud shadow detection in Landsat imagery". *Remote Sensing of Environment*, 118(C), 83–94. doi:10.1016/j.rse.2011.10.028.